Rensselaer

DEPARTMENT OF MECHANICAL, AEROSPACE, AND NUCLEAR ENGINEERING

"CFD MODELING: AIRFOIL ON MARS IN ACUSOLVE"

Batuhan Yalcin, Charles Carrillo, Demetrius Walker

2409 INTRO COMPUTATIONAL FLUID DYNAMICS

[2409 MANE 6140 01]

Final Paper

Tuesday, November 26th, 2024

Table of Contents

Table of Figures

List of Tables

Table of Equations

Section 1: Overall Description of the Problem (Charles 33%, Batuhan 33%, Demetrius 33%)

Background

Visiting distant planets used to be something only possible in science fiction movies like *Star Wars* and *Star Trek*. However, with modern technology, visiting far-off planets is now within reach and could happen soon. Mars is intriguing for several reasons. It is one of the closest planets to Earth, making it a natural first choice for exploration. Additionally, Mars is believed to have been much like Earth, raising the possibility that it may have supported ancient life. NASA administrator Steve Jurczyk notes that "Mars is the most Earth-like planet in our solar system." [1] As Mars continues to captivate scientists, vehicles capable of navigating its unique atmosphere and terrain are critical. In the past, rovers were sent to Mars to collect surface data and imagery. Most recently, the Mars 2020 Perseverance Rover was deployed to search for signs of microscopic life. [2]

The next step in Mars exploration is to send small aircraft like drones or UAVs (Unmanned Aerial Vehicles). In 2021, the Mars Ingenuity Helicopter landed on Mars and performed 72 successful sorties in support of the Perseverance mission, gathering vital data on flight dynamics on Mars. The future goal is to deploy larger, more efficient aircraft to Mars. A

small UAV like the RQ-11 can travel much faster and more efficiently than the Ingenuity Helicopter due to its ability to perform winged flight. [3] A study on how the differences in Mars' atmosphere effect on the generation of lift, drag, and aerodynamic moments on aircraft could provide valuable insights for designing future UAVs to fly through the Martian sky.

Geometry

The NACA 2412 airfoil was selected due to its common use in small UAVs and the extensive CFD modeling available for it, which allows for effective benchmarking. An image of the NACA 2412 is shown in Figure 1. A chord length of 1 meter was chosen initially to model the upper limit of UAVs that might be chosen to fly in the Martian atmosphere. For the final presentation, similar geometry with adjusted chord length will be used to fill a flight envelope for SUAVs in the Martian atmosphere.

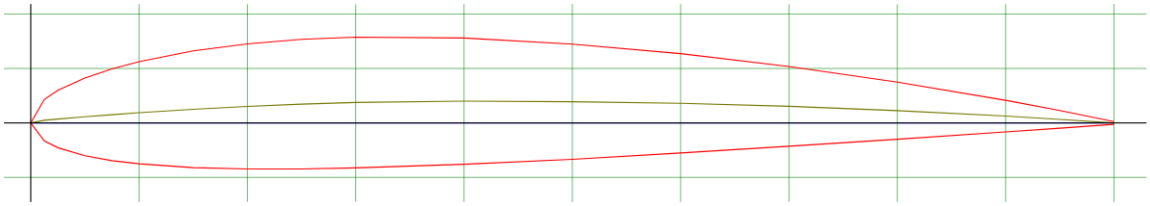

Figure 1: NACA 2412 [4]

Equations Involved

Both the Reynolds Number and Mach number will be especially important values when attempting to model flight in Mars' atmosphere. The equations for both are as follows:

Equation 1: Reynold Number Calculation

$$Re = \frac{\rho * V * L}{\mu}$$

The variable V represents the free stream velocity, ρ the atmospheric density, L the chord length, and μ the air viscosity.

Equation 2: Mach Number Calculation

$$Mach = \frac{V}{a}$$

The variable V represents free stream velocity and, a being the speed of sound.

The next following equations are important in the development of the flight envelope. The equations are as follows:

Equation 3: Temperature at Specific height

$$T = T_0 - \Gamma * h$$

The variable T_0 represents the surface temperature, Γ represents the temperature lapse rate, and h represents the altitude

Equation 4: Density at Specific height using temperature

$$\rho = \rho_0 * \left(\frac{T}{T_0}\right)^{\frac{g*M}{R*\Gamma}-1}$$

The variable ρ_0 represents the surface density, Γ represents the temperature lapse rate, T_0 represents the surface temperature, g represents the gravity, M represents the atmospheric molar mass, R represents the atmospheric gas constant, and h represents the altitude.

Equation 5: Maximum Lift from Material Strength

$$\sigma * A = Lift$$

The yield strength, σ, multiplied by area, A, is the maximum amount of lift that a wing can sustain without bending.

Equation 6: Maximum Thrust from Material Strength

$$Thrust = 0.5 * \rho * V^2 * C_D * A = 1.75 * W$$

The maximum thrust that can be produced cannot surpass a factor of 1.75 times the weight, W of the wing because the drag forces would be too much for the blade to handle.

Equation 7: Maximum Thrust from Power Capacity

$$Thrust * V = 0.5 * \rho * V^3 * C_D * A = Power$$

The maximum thrust can also be calculated by the limit of power that the battery can produce.

Equation 8: Stall Speed

$$Stall\ Speed = \sqrt{\frac{2 * W}{\rho * S * C_L}}$$

The stall speed is the minimum speed needed for the aircraft to overcome its own weight. Going below this value will result in loss of control and likely system failure. It is dependent on both environmental properties like density and vehicle properties like wing area, S and weight.

Equation 9: Load Factor

$$Load\ Factor = \frac{L}{W}$$

The load factor is the amount of lift being generated per weight of the wing. It is an important ratio used in determining stall acceleration.

Equation 10: Stall Acceleration

$$Stall\ Acceleration = Stall\ Speed * \sqrt{Load\ Factor}$$

The stall acceleration is the change in stall velocity due to the increase in lift relative to the weight. The stall acceleration will set the maximum for velocity before other types of failure such as battery limitations and material strength.

The drag coefficient, C_D, is a dimensionless number that aerodynamicists use to account for the complex factors affecting drag, such as shape, inclination, and certain flow conditions. It is derived from the drag equation by solving for C_D. Mathematically, the drag coefficient is expressed as:

Equation 5: C_D Calculation

$$C_D = \frac{D}{\rho A\, V^2/2}$$

The variable D is the drag force, ρ is the fluid density, V is the velocity of the object relative to the fluid, and A is the reference area. Thus, C_D is the drag divided by the product of the density, half the velocity squared, and the reference area.

Equation 6: C_L Calculation

$$C_L = \frac{L}{\frac{1}{2}\rho U_\infty^2 bc}$$

The variable C_L is the coefficient of lift, which is determined by the type of airfoil and angle of attack. L is the lift, which must equal the airplane's weight in kilograms, ρ is density of the air, U_∞^2 is the velocity expressed in meters per second and bc is the wing area of an aircraft in square feet

Material Inputs

The main challenge in modeling an airfoil on Mars is the significant difference in key atmospheric properties. Earth's atmosphere is primarily composed of nitrogen, while Mars' atmosphere consists mostly of carbon dioxide [1]. A table of the major differences in properties is provided in Table 1.

Properties	Mars	Earth
Gravity [m/s^2]	3.71	9.81
Atmospheric Temperature [K]	210	288
Air Density [kg/m^3]	0.020	1.225
Air Viscosity	1.37e-5	1.81e-5

Atmospheric Gas Constant	192	287
Atmospheric Molar Mass [g/mol]	43.34	28.97
Temperature Lapse Rate [K/km]	4.5	6.5

Table 1: Atmospheric Properties on Earth and Mars [1]

Conditions

The airfoil will be tested at various velocities in both Martian and Earth's atmospheres. Initially, the Reynolds number will be set to 100,000 for both environments, corresponding to a Mach number of 0.00565 on Earth and 0.285 on Mars. To develop a comprehensive flight envelope, a range of velocities will be analyzed. The corresponding Reynolds and Mach numbers are presented in Table 2.

Mars			Earth		
Velocity	Reynolds Number	Mach Number	Velocity	Reynolds Number	Mach Number
27.6	39,428	0.115	27.6	1,867,956	0.080
50	71,429	0.208	50	3,383,978	0.146
75	107,143	0.313	75	5,075,967	0.219
125	178,571	0.521	125	8,459,945	0.364
175	250,000	0.729	175	11,843,923	0.510
225	321,429	0.938	225	15,227,901	0.656

Table 2: Mars and Earth Conditions

Section 2: Assumptions and Problem Setup (Charles 33%, Batuhan 33%, Demetrius 33%)

Physics Modeled

For the midterm report, the physical model will be simple. A laminar flow assumption will be applied to a mesh designed to capture turbulent flows, and the simulation will use steady-state, single phase conditions. Additionally, the model will be treated as two-dimensional to further simplify the analysis, and three-dimensional for the further flow pattern analysis.

Boundary Conditions

For 2D, the simulation utilized specific boundary conditions to properly simulate an airfoil. A no-slip wall condition was applied to the inner surface of the airfoil, ensuring that the velocity at the wall is zero. A slip wall condition was used at the edge of the airfoil and along the surface of the airfoil boundary, allowing flow along the skin of the airfoil. No symmetry conditions were applied, and a far-field boundary was set with varying velocities.

For 3D, the Immersed Boundary (IB) method is utilized within the Lattice Boltzmann Method (LBM) to handle complex or moving boundaries. The logic of the IB method involves applying forces at boundary nodes to create a "no-slip" effect or to achieve the

desired boundary condition. These forces adjust the fluid velocities to align with the velocities of the immersed boundary, enabling accurate representation of fluid-structure interactions. This method is particularly effective for simulating flows around intricate geometries and dynamic structures within a uniform lattice.

In 3D, Open boundary conditions are implemented to support both inflow and outflow scenarios. These conditions ensure smooth entry and exit of the fluid domain without artificial reflections or disruptions, maintaining the integrity of the flow simulation.

Also, in 3D the bounce-back mechanism is employed to enforce no-slip conditions at solid boundaries. In this approach, fluid particles are reflected back with reversed velocities at the boundary, ensuring that the fluid velocity relative to the boundary surface is zero. This is crucial for simulating stationary or solid boundaries accurately. It used for the landing simulation

Section 3: Numerical Scheme and Mesh Setup (Charles 33%, Batuhan 33%, Demetrius 33%)

Numerical Scheme

For the 2D simulations, the default settings of Altair HyperMesh CFD 2024.0.0.27 were applied. For the 3D simulations, the LBM (Lattice Boltzmann Method) was used. The reason for selecting LBM is that it is particularly suitable for low Mach number flows, where our Mach number remains well below 1. Additionally, LBM is highly efficient for GPU-based parallel programming, allowing us to run 30 million mesh cells in real time. Another advantage is that it is one of the most accurate schemes for low Mach number flows and complex geometries.

Mesh Setup

In addition to the surface and volume mesh, a box was added around the airfoil. This method was chosen because the flow behavior around the airfoil is more critical than in the rest of the volume domain. For the volume and surface mesh creation, the mesh size method used a maximum element size of 0.254. Curvature-based surface refinement was applied, with a minimum size factor of 0.1. A geometric feature angle of 22.5 was used, with a mesh growth rate of 1.3. Boundary layers were generated only on fluid domains. The element size of the box was varied in each simulation, ranging from 1.984375 to 0.005953125 meters for a 1-meter chord length. For the benchmark comparison with the airfoil at a 0.1-meter chord length, the box element size was set to 0.00039 meters to achieve an optimal mesh count of around 160,000.

Section 4: Run Setup and Refinement (Charles 33%, Batuhan 33%, Demetrius 33%)

Run Plan

The run plan consists of three parts for both the Martian and Earth conditions. We wanted to capture data to ensure that our model is consistent with our benchmark data, run simulation values against theoretical values for the flight envelope and model this using a 3D Lattice-Boltzmann Model. For the clarity of this section, the tables with data for each set of runs can be found in section 5.

1. Run set one consists of 26 runs, 13 for each atmospheric condition, with a Reynolds number of 100,000, covering angles of attack from negative 30 degrees to 30 degrees in 5-degree increments. For the purposes of analyzing the flow alone we decided to omit the initially contemplated heat-transfer.

2. Run set two consists of 12 runs, 6 for each atmosphere at the minimum, maximum and some intermediate values determined from the analytical flight envelope. Initially, we wanted to test for several angles of attack for each speed, however we found that such data was not going to be pertinent to the creation of the flight envelope, since for that we are considering steady-level flight.

3. For our 3D visualization, we simulated a soft landing at 2 m/s, minimum and maximum flight speed limits in each atmosphere. We added more fidelity by adding a solid boundary near the geometry to simulate the air between the ground and the airfoil for the moment of landing.

Run Setup

Single-phase, incompressible, steady flow was assumed. The Spalart-Allmaras turbulence model was used, as specified for the midterm paper. Transition effects were not considered, and gravitational acceleration differences were excluded from the Acusolve analysis. However, gravity is a consideration when building the flight envelope's left and right limits.

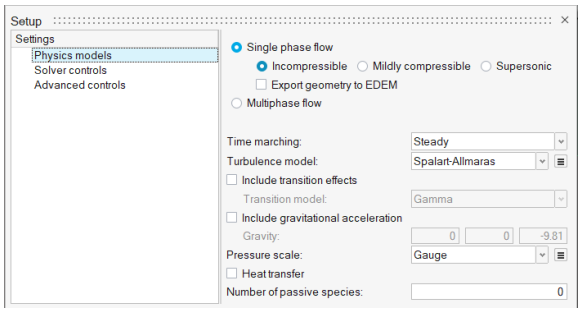

Figure 2: Physics setup of the flow

A velocity far field is applied as in the previous report. The velocity was changed accordingly throughout the different runs to acquire benchmark data at different angles of

attack using trigonometric vector relationships to calculate v_x and v_y values. ($v_x = v \cos(\theta)$ and $v_y = v \sin(\theta)$)

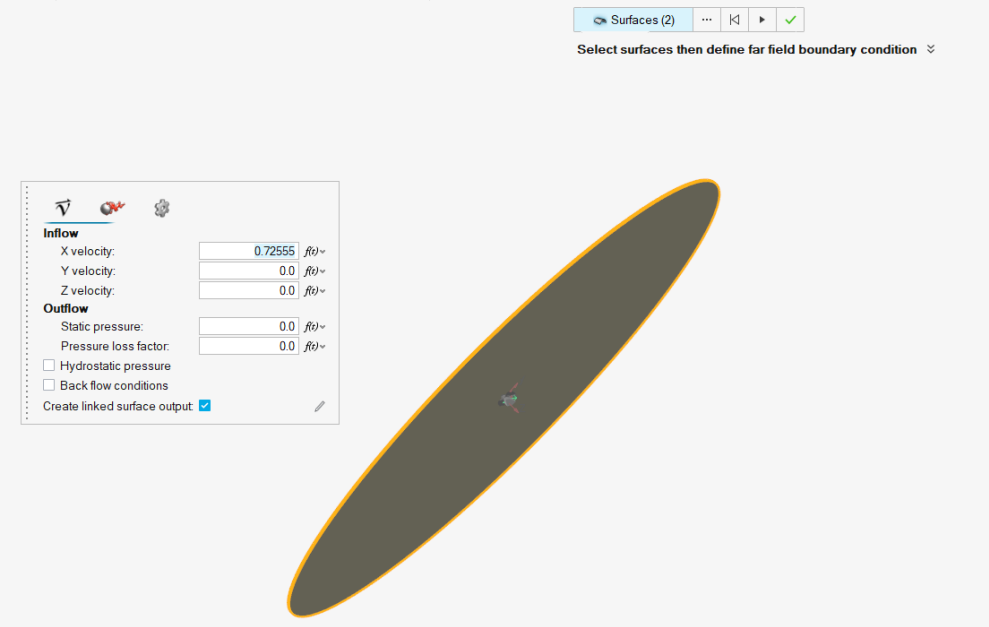

Figure 3: Far Field Applied as 0.7255 in x axis for the velocity stream

For the run and restart method, all processes were executed using serial processing without MPI. Each problem was solved with a unique suffix, while the working directory remained the same. For each new run, only the problem suffix was changed, allowing it to continue from the previous state. Time steps were restarted to obtain more accurate results.

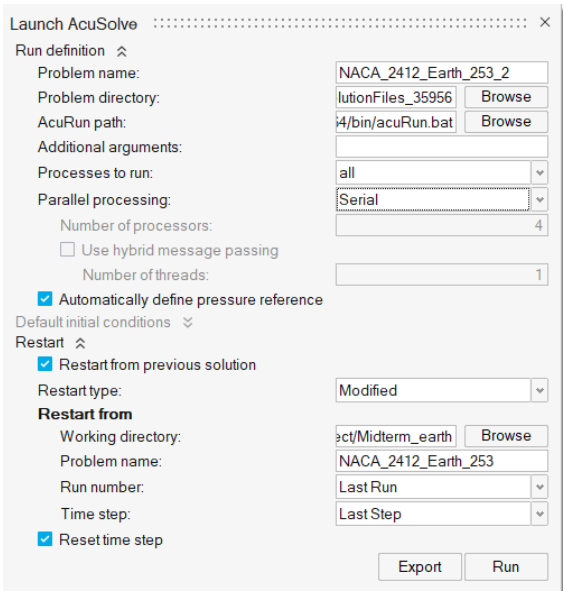

Figure 4: Run and Restart Strategies

Mesh Refinements

The initial mesh elements required refinement to accurately capture the effects of the airfoil in different atmospheres. We conducted a grid refinement study to ensure accuracy in future solutions. For the benchmark case, the final error was 0.47% at the benchmark chord length, indicating that a mesh with approximately 157,000 control volumes provides an excellent estimate for our current geometry and setup. Two tables comparing different numbers of control volumes are shown below.

Mesh	# CVs	Run Time	C_L	C_D
Mesh_0_Earth	17672	2 minutes	0.002595	0.0012708
Mesh_1_Earth	48000	4 minutes	0.0020234	0.0018289
Mesh_2_Earth	161740	24 minutes	0.0019639	0.0015724
Mesh_3_Earth	173408	10 minutes	0.0019597	0.0015

Table 3: Mesh refinement table for the Earth atmosphere

Mesh	# CVs	Run Time	C_L	C_D
Mesh_0_Mars	17672	2 minutes	0.095427	0.046063
Mesh_1_Mars	48000	4 minutes	0.07352	0.064726
Mesh_2_Mars	161740	24 minutes	0.071596	0.058724
Mesh_3_Mars	173408	10 minutes	0.07234	0.054128
Mesh_4_Mars	253700	20 minutes	0.078539	0.49382
Mesh_5_Mars	759492	More than 2 hours	N/A	N/A

Table 4: Mesh refinement table for the Mars atmosphere

After approximately 175,000 control volumes, the values show minimal variation, indicating that mesh convergence has been achieved. This stability suggests that further increases in mesh density are unlikely to yield significant improvements in accuracy for the current model.

Mesh	# CVs	Run Time	C_L Benchmark	C_D Benchmark	C_L CFD	C_D CFD	C_L Error
0.1-meter Cord Length	157508	14 minutes	0.211	0.0211	0.212	0.0263	%0.47

Table 5: Comparing our optimum mesh with the benchmark data

We scaled down the geometry to match the benchmark data and achieved a margin of error below 1%. Some errors are expected due to the simplified and low-detail geometry created for the simulation as well as due to the increase in the chord length.

.

Details

Airfoil: NACA 2412 (naca2412-il)
Reynolds number: 50,000
Max Cl/Cd: 34.64 at α=6.5°
Description: Mach=0 Ncrit=5
Source: Xfoil prediction
Download polar: xf-naca2412-il-50000-n5.txt
Download as CSV file: xf-naca2412-il-50000-n5.csv

Polar file

-1.000	0.0749	0.02117	0.01169	-0.0476	0.9291	1.0000
-0.750	0.1092	0.02114	0.01148	-0.0495	0.9152	1.0000
-0.500	0.1437	0.02113	0.01132	-0.0513	0.9017	1.0000
-0.250	0.1775	0.02111	0.01117	-0.0527	0.8883	1.0000
0.000	**0.2112**	**0.02110**	**0.01104**	**-0.0540**	**0.8752**	**1.0000**
0.250	0.2457	0.02106	0.01091	-0.0553	0.8626	1.0000
0.500	0.2790	0.02102	0.01079	-0.0562	0.8497	1.0000
0.750	0.3077	0.02104	0.01074	-0.0563	0.8350	1.0000
1.000	0.3361	0.02107	0.01071	-0.0562	0.8203	1.0000
1.250	0.3643	0.02111	0.01070	-0.0560	0.8056	1.0000
1.500	0.3924	0.02116	0.01071	-0.0558	0.7908	1.0000
1.750	0.4206	0.02122	0.01073	-0.0555	0.7761	1.0000
2.000	0.4485	0.02128	0.01076	-0.0552	0.7613	1.0000
2.250	0.4763	0.02135	0.01081	-0.0548	0.7464	1.0000
2.500	0.5037	0.02144	0.01088	-0.0543	0.7313	1.0000
2.750	0.5306	0.02155	0.01097	-0.0537	0.7159	1.0000

Figure 5: Benchmark data of NACA 2412

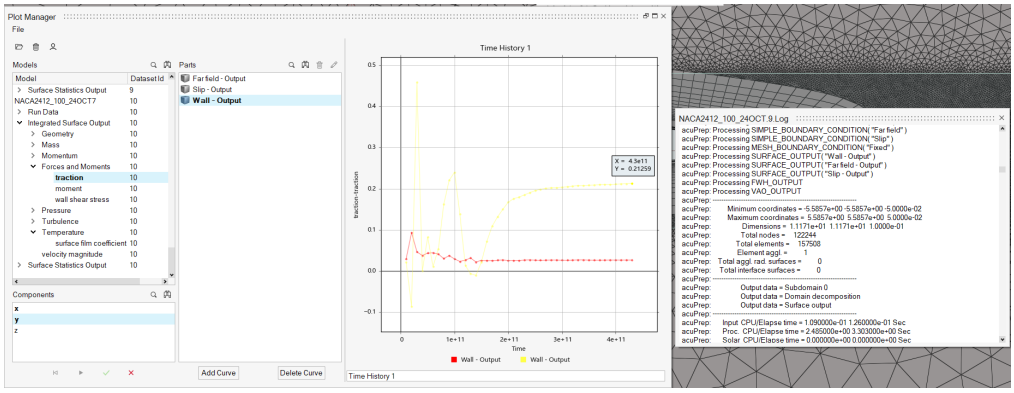

Figure 6: CFD results of the NACA 2412 airfoil with 0.1 m cord length in comparison to benchmark.

For mesh refinement, we chose a box refinement to get a clearer view of what was happening around the airfoil. By changing the element size within this box, the number of control volumes (CVs) increased, focusing refinement on the flow around the airfoil, which is more critical than the rest of the domain. For volume and surface mesh creation, a maximum element size of 0.254 was used. Curvature-based surface refinement was applied with a minimum size factor of 0.1. A geometric feature angle of 22.5 was set, with a mesh growth rate of 1.3. Boundary layers were generated only on fluid domains. The element size within the box varied in each simulation from 1.984375 to 0.005953125 meters.

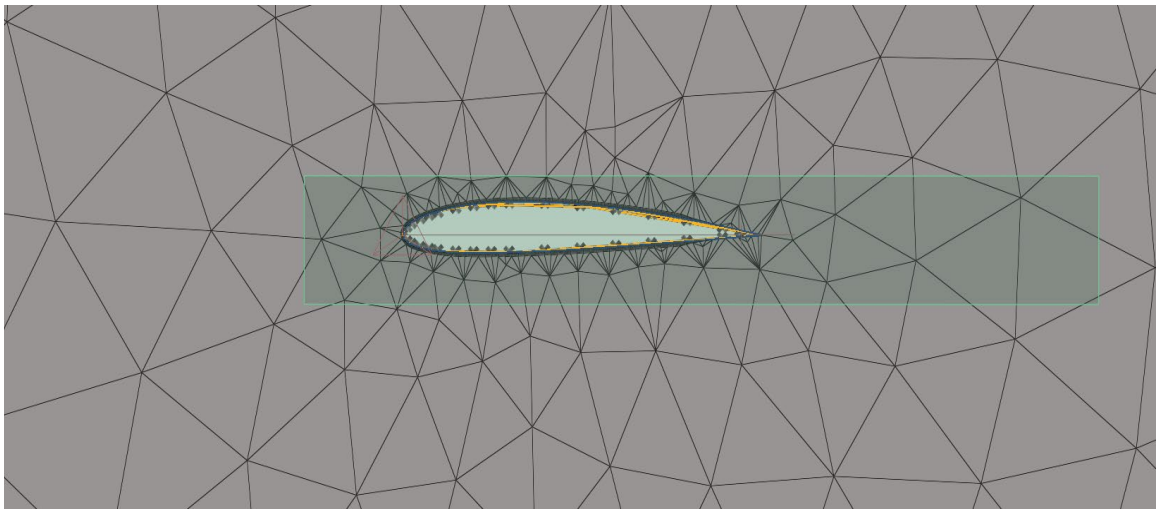

Figure 7: Maximum number of mesh elements tested. 253700 CVs.

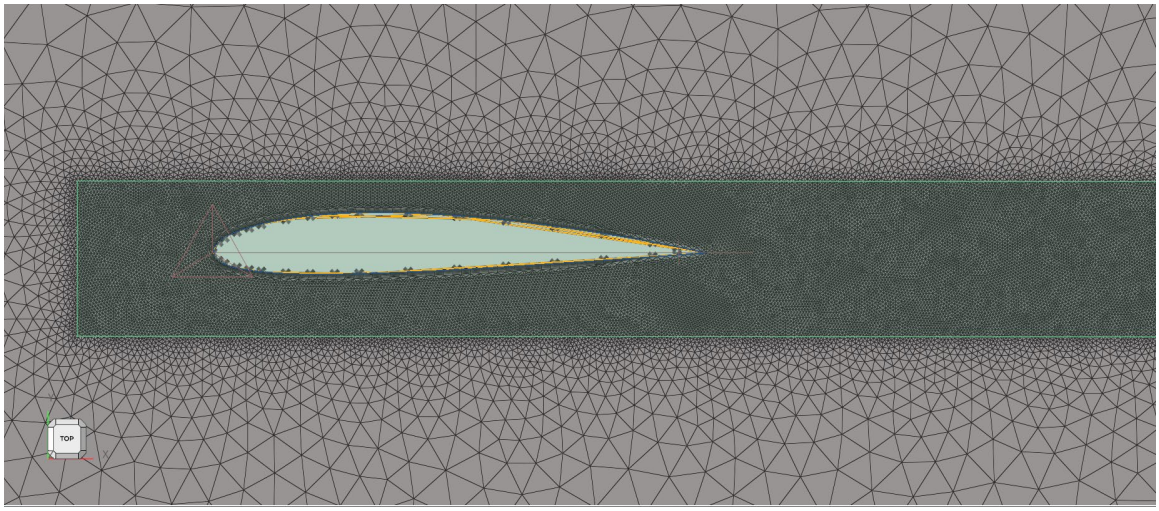

Figure 8: Maximum number of mesh elements tested, 253700 CVs. Zoomed out version

Section 5: Post-Processing and Results (Charles 33%, Batuhan 33%, Demetrius 33%)

Benchmark Data Comparison via Different Angles of Attack (Run Set One)

Our first set of simulations was conducted to evaluate our model against the benchmark data with greater fidelity. The Reynolds number was kept constant at 100,000 to keep the same turbulence model and to mirror the benchmark data conditions.

Planet	Mesh#	Re	Mach	Velocity	Angle of Attack	Cl	Cd
Earth	48	100,000	0.005655431	1.51	30	0.0952	0.00158
Earth	48	100,000	0.005655431	1.51	25	0.0876	0.00239
Earth	48	100,000	0.005655431	1.51	20	0.082	0.00316
Earth	48	100,000	0.005655431	1.51	15	0.069	0.0037
Earth	48	100,000	0.005655431	1.51	10	0.059	0.0046
Earth	48	100,000	0.005655431	1.51	5	0.0392	0.0058
Earth	48	100,000	0.005655431	1.51	0	0.00875	0.00706
Earth	48	100,000	0.005655431	1.51	-5	-0.0232	0.0073
Earth	48	100,000	0.005655431	1.51	-10	-0.045	0.00732
Earth	48	100,000	0.005655431	1.51	-15	-0.0539	0.00747
Earth	48	100,000	0.005655431	1.51	-20	-0.0635	0.007156
Earth	48	100,000	0.005655431	1.51	-25	-0.0749	0.00676
Earth	48	100,000	0.005655431	1.51	-30	-0.084	0.006

Table 6: Earth Run Plan at Reynolds Number of 100,000 with Varying Angles of Attack

Planet	Mesh#	Re	Mach	Velocity	Angle of Attack	Cl	Cd
Mars	48	100,000	0.285416667	68.5	30	3.2129	0.0563
Mars	48	100,000	0.285416667	68.5	25	2.966	0.0737
Mars	48	100,000	0.285416667	68.5	20	2.7741	0.0987
Mars	48	100,000	0.285416667	68.5	15	2.361	0.13
Mars	48	100,000	0.285416667	68.5	10	1.997	0.158
Mars	48	100,000	0.285416667	68.5	5	1.32	0.195
Mars	48	100,000	0.285416667	68.5	0	0.2921	0.24088
Mars	48	100,000	0.285416667	68.5	-5	-0.787	0.2486
Mars	48	100,000	0.285416667	68.5	-10	-1.42	0.244
Mars	48	100,000	0.285416667	68.5	-15	-1.825	0.25538
Mars	48	100,000	0.285416667	68.5	-20	-2.182	0.02453
Mars	48	100,000	0.285416667	68.5	-25	-2.516	0.229
Mars	48	100,000	0.285416667	68.5	-30	-2.837	0.20411

Table 7: Mars Run Plan at Reynolds Number of 100,000 with Varying Angles of Attack

Benchmark Comparison

Using the airfoil tools [7] benchmark data for the NACA 2412 airfoil, we compared the results with our CFD simulations. The benchmark data included 96 different angles of attack, which was not time-feasible to run for all cases in our setup. Therefore, we conducted simulations for angles ranging from -30° to 30° in 5° increments. To align our results with the 96-point benchmark data, we used Python's polyfit function to fit an 11th-degree polynomial. In addition, we supplement this with a raw data plot in MATALAB using a normalization technique. Normalization in the MATLAB plots are used in order to account for scaling issues with chord length and values obtained via the different atmospheres.

Our primary simulations were performed on a NACA 2412 airfoil with a chord length of 1 meter. However, to match the benchmark data and validate our setup further, we had to create a 0.1-meter chord length airfoil and to adequately capture the benchmark data cases.

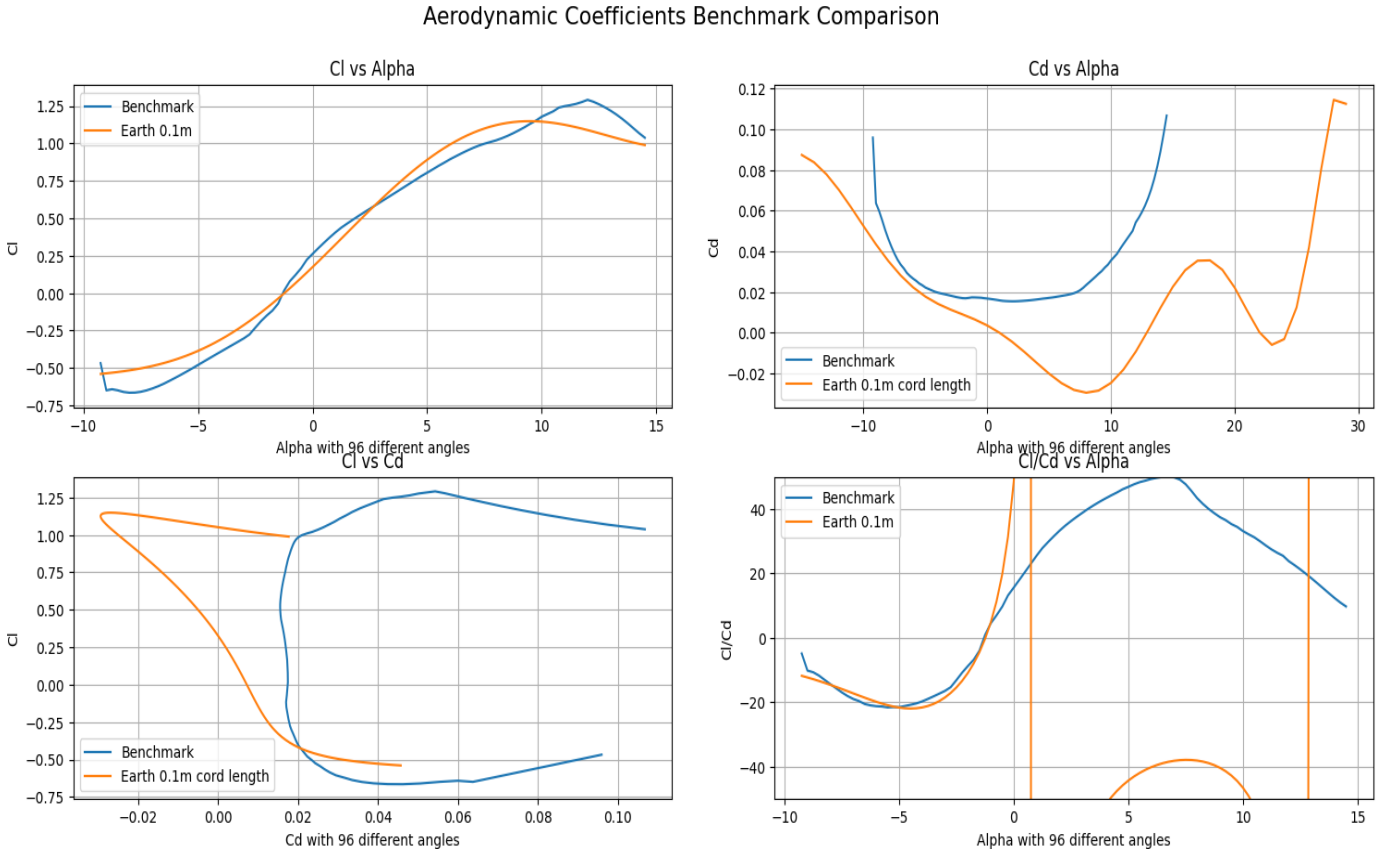

Figure 9: Benchmark Comparison with 0.1-meter cord length [7].

The results show that while our data is rather accurate for C_L, we encountered accuracy issues with C_D, suggesting a potential problem with the airfoil geometry or the testing setup in Acusolve. Since C_D is sensitive to the surface properties of the airfoil and the quality of its design, these issues could have contributed to the discrepancies. Our geometry creation

process involves defining discrete points along the airfoil and connecting them with lines to form its curvature. However, this method is not sufficiently refined for a large airfoil, such as the one-meter chord length used in our simulations. Accurately representing the airfoil at this scale likely requires thousands of points to achieve a smoother and more precise geometry. The Cl/Cd vs alpha graph is particularly questionable, and more work needs to be done to identify the issues therein.

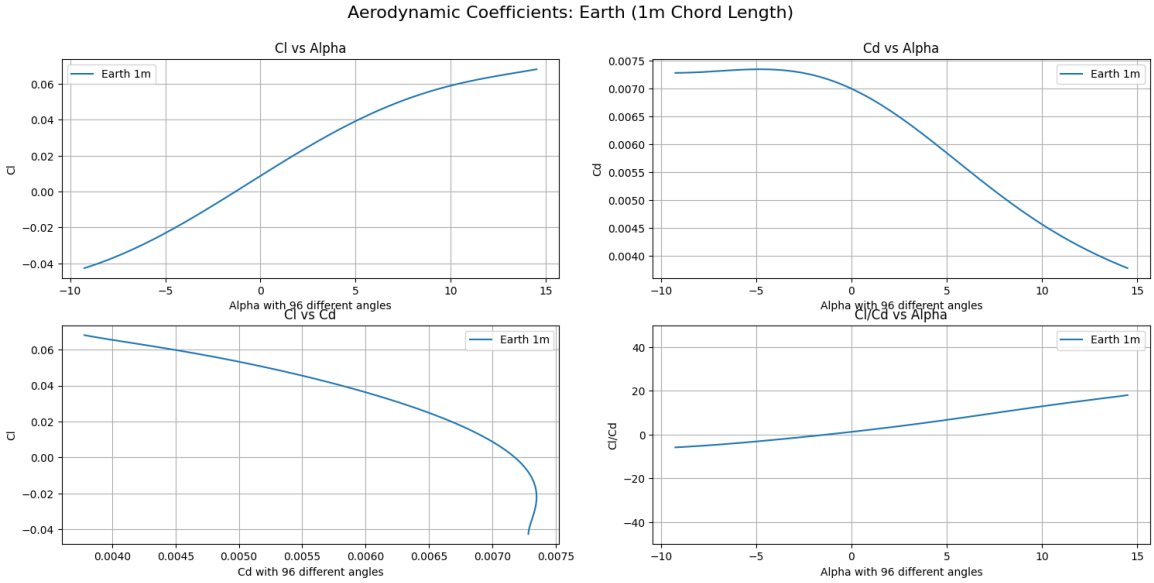

Figure 10: Aerodynamic coefficients CL and CD for Earth atmosphere using 1m Chord length.

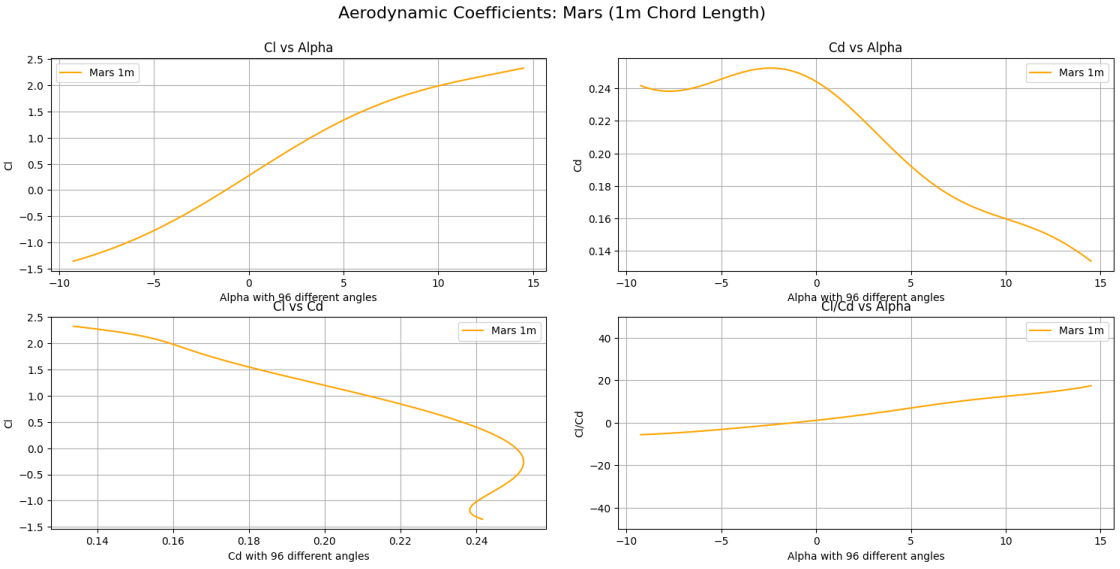

Figure 11: Aerodynamic coefficients CL and CD for Martian atmosphere using 1m Chord length.

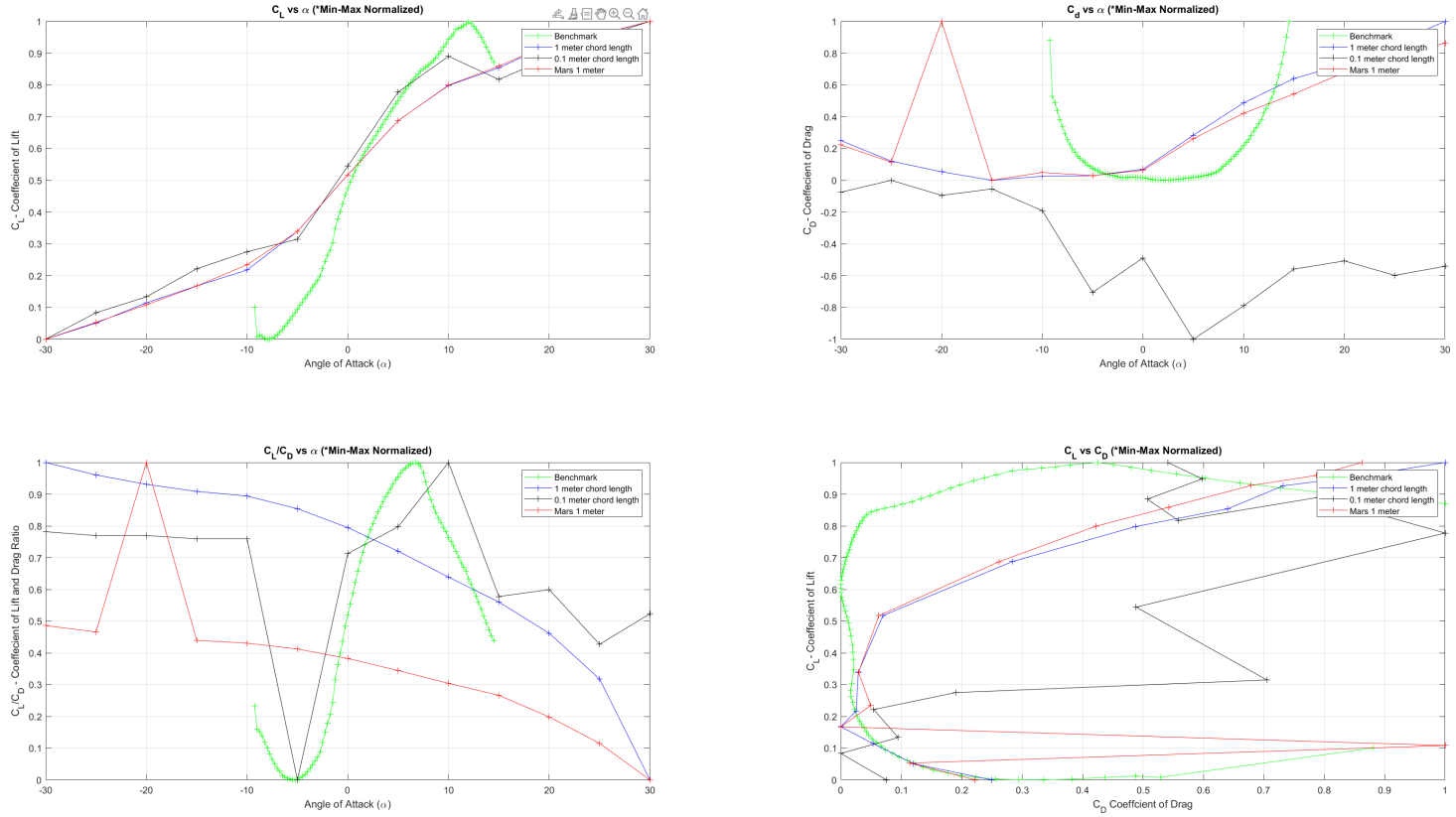

Figure 12: Raw MATLAB Total Aerodynamic coefficients comparison between Earth, Martian and Benchmark atmosphere scaled via a min-max technique to account for scale differences

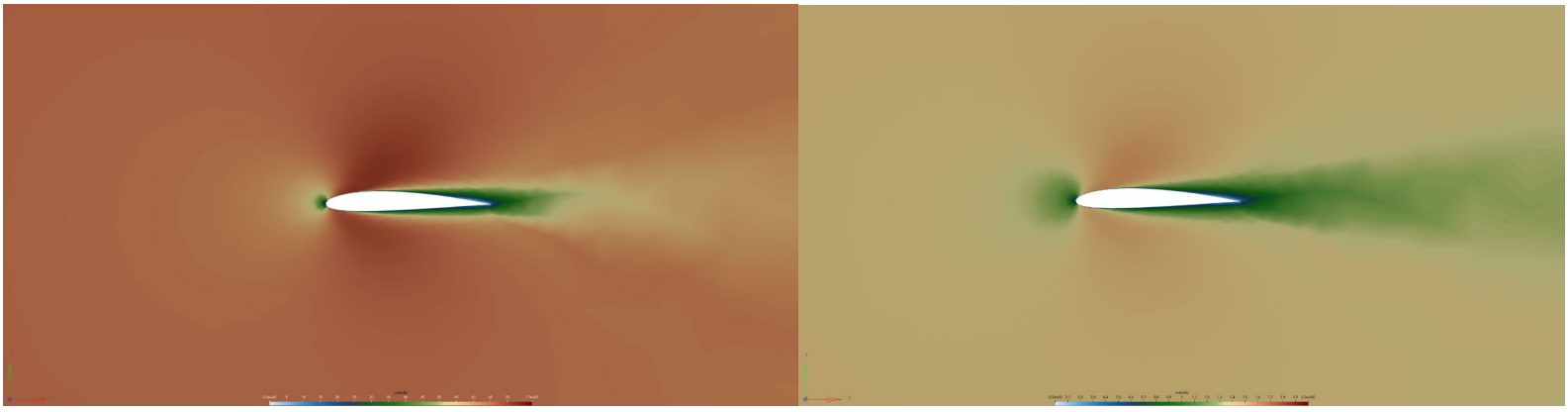

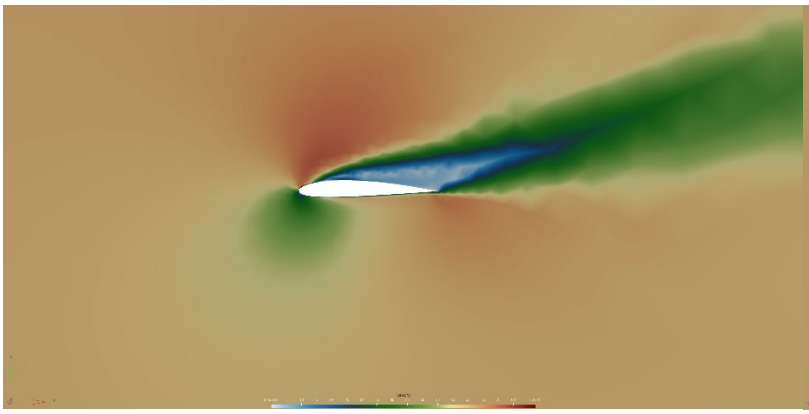

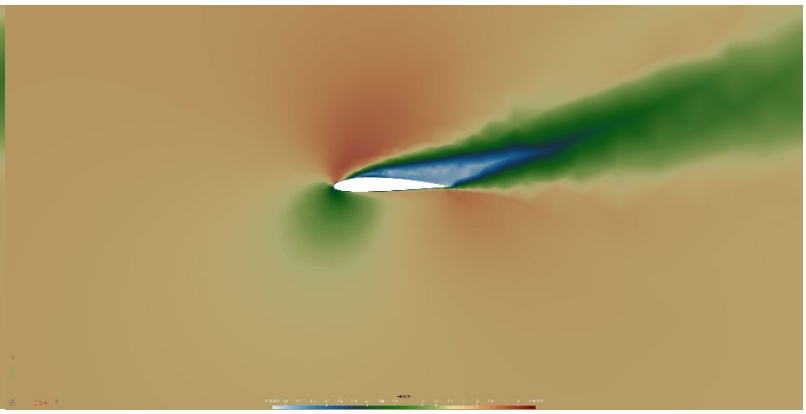

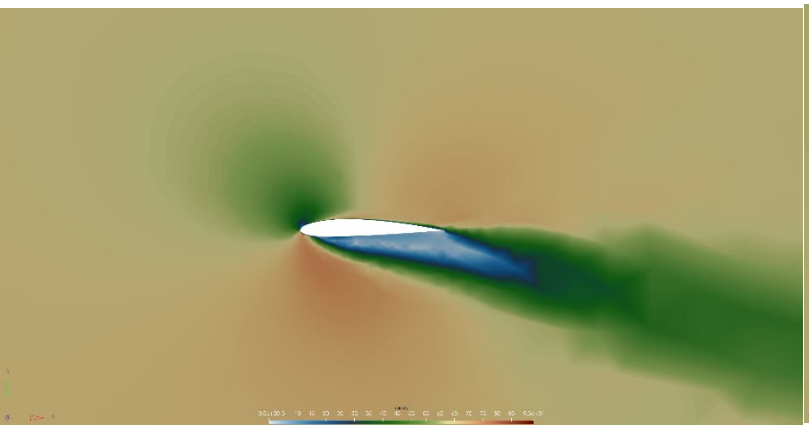

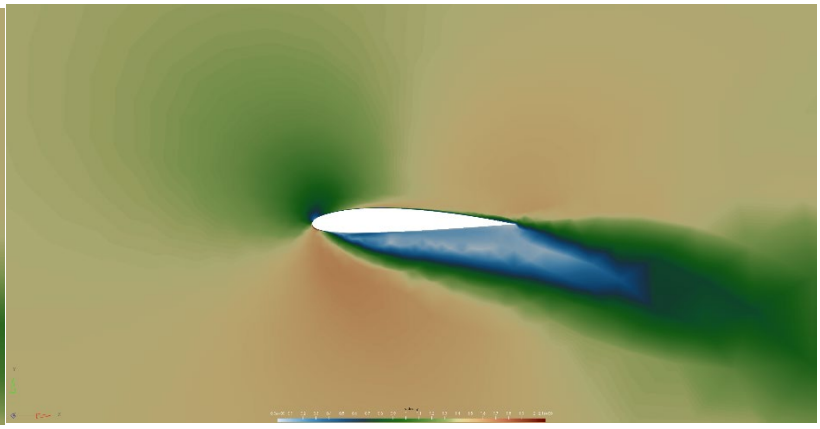

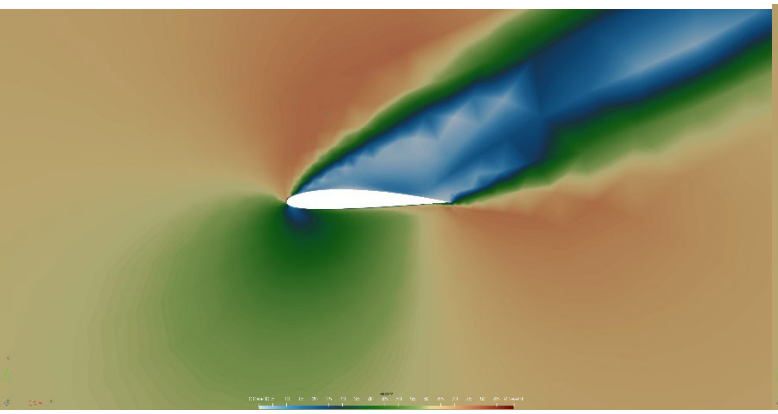

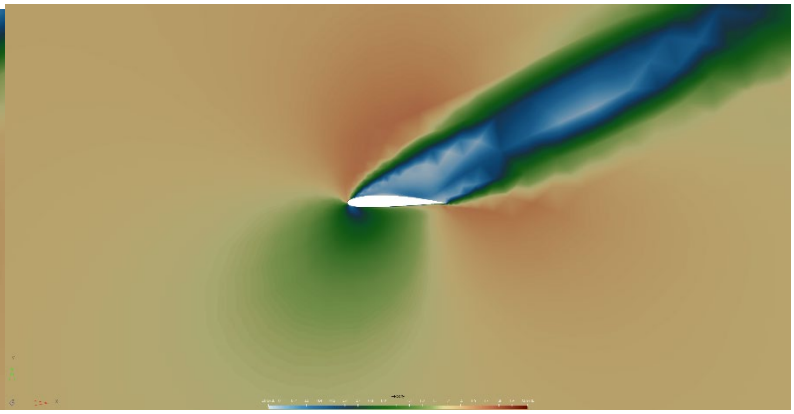

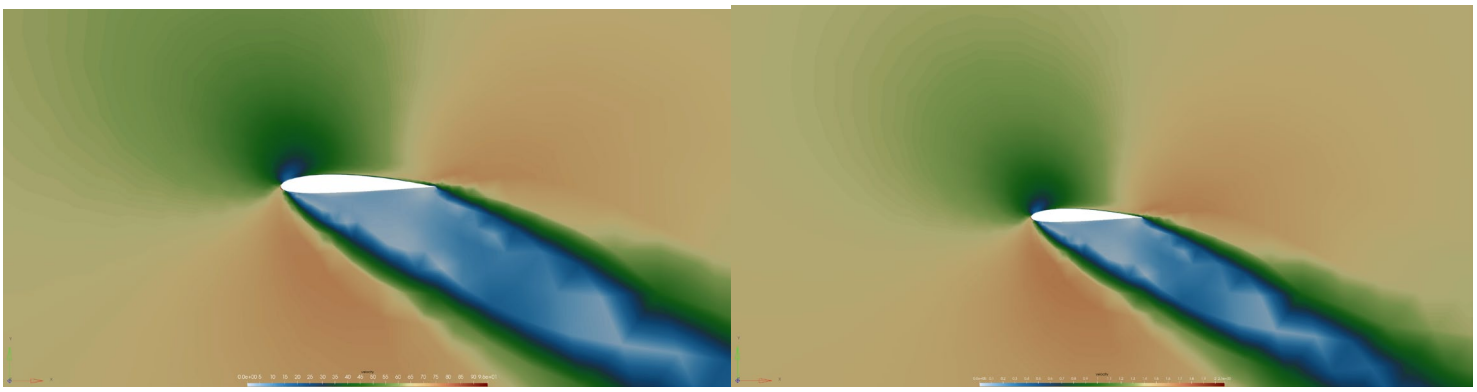

Figure 13a: Depicts the resulting flow patterns for Mars (left) Earth (Right) for 0, 15,-15,30 and -30 degree angles of attack

The results show that while C_L and C_D differ significantly between Earth's and Mars' atmospheres, both are higher in the Martian atmosphere due to the higher viscosity caused by the CO_2-dominated composition. However, the C_L/C_D ratio remains nearly the same when comparing the two planets. The data in many instances does not quite match the benchmark data but rather roughly outlines it. Especially, when we look at the data in a normalized fashion (figure 10), it is once again reinforced that our Lift coefficient data is quite accurate but we lack fidelity in the other three plots due to our discrepancy in the Drag coefficient. If there was more time, we would match the angles of attack by degree to the benchmark case and pay special attention to what's happening at the boundary layers for our airfoil to determine Acusolve's approximation of the coefficient of drag. Something is clearly not right, which is skewing our data quite a bit. Regardless of the discrepancy, we can see clearly that the Mars and Earth data for the same chord length behaves similarly yet scaled differently due to the effects of their atmosphere.

The effect of angle of attack on the coefficients of lift and drag is observed to be similar, with the coefficient of lift increasing by a factor of ten when the angle of attack is raised from 0 to 25 degrees. The results indicate that the angle of attack influences lift and drag in the same manner in both atmospheres. However, the thinner Martian atmosphere enables the aircraft to achieve higher speeds while maintaining the same Reynolds number as on Earth.

Flight Envelope Development (Run Set Two)

A flight envelope is a graphical representation of an aircraft's operational limits. It typically illustrates the minimum and maximum speeds at which the aircraft can safely operate

under varying conditions, such as altitude and load factor. These speed limits are influenced by factors including material strength, aerodynamic design, and energy constraints, such as battery capacity. An example of a flight envelope is shown below in Figure 13.

Case Run Plan Flight Envelope						
Planet	Mesh#	Re	Mach	Velocity	Cl	Cd
Earth	173	1,829,834	0.080466	27.6	2.947	1.4644
Earth	173	3,314,917	0.145773	50	8.966	4.9475
Earth	173	4,972,376	0.218659	75	24.035	10.588
Earth	173	8,287,293	0.364431	125	58.879	31.1
Earth	173	11,602,210	0.510204	175	125.54	63.22
Earth	173	14,917,127	0.655977	225	184.34	94.906
Mars	173	402,920	0.115	27.6	0.0411	0.0337
Mars	173	729,927	0.208333	50	0.16	0.108
Mars	173	1,094,891	0.3125	75	0.3802	0.2416
Mars	173	1,824,818	0.520833	125	1.0784	0.6329
Mars	173	2,554,745	0.729167	175	2.224	1.155
Mars	173	3,284,672	0.9375	225	3.45	1.897

Table 8: Run Plan two for flight envelope spectrum analysis

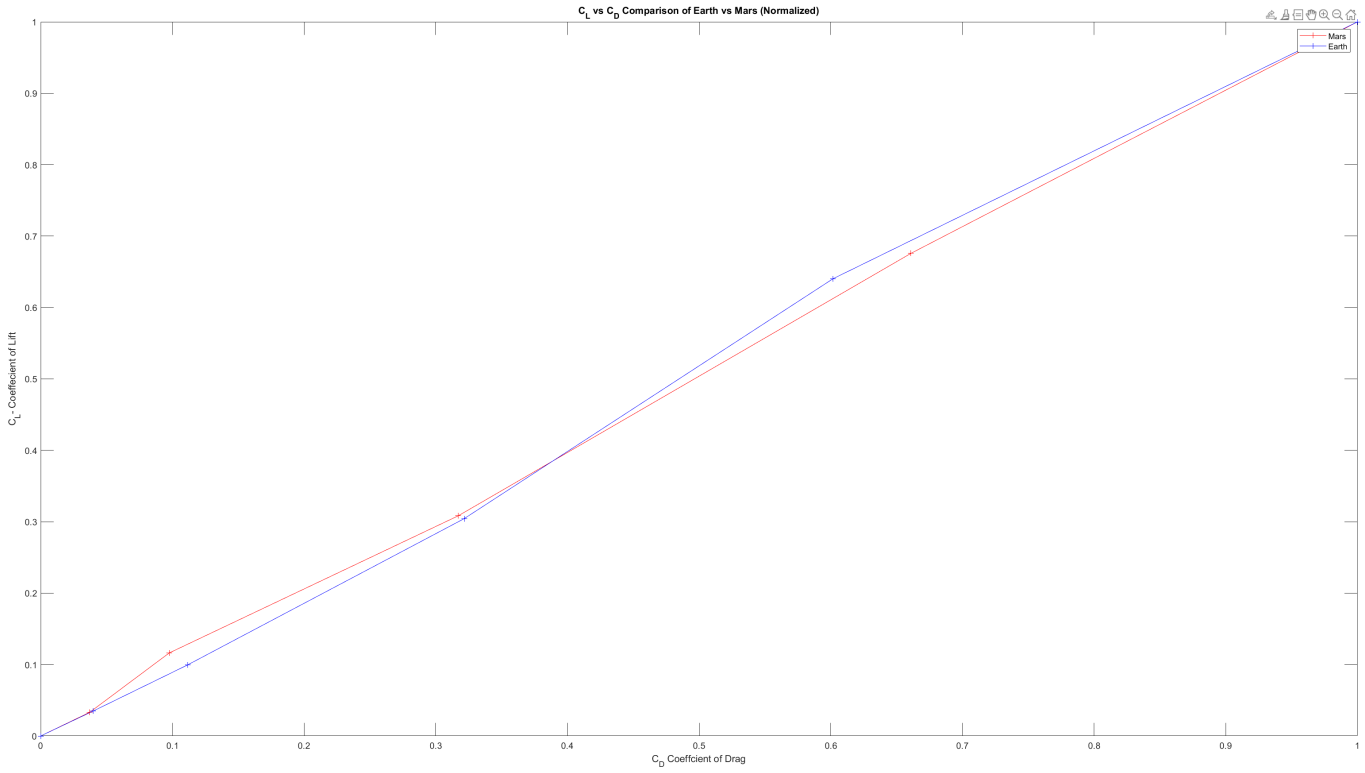

Figure 13: MATLAB comparison of flight envelope spectrum for Mars and Earth.

The first key insight is that every time this data needs to be compared, it must be normalized. If they are presented prior to being normalized they will have little discernible meaning due to the scaling differences as seen in Table 8. We can see that their behavior naturally mimics each other, linearly as speed increases and atmospheric conditions remain the same. The raw graph shows values for Mars increasing on an exponentially smaller scale indicating that it is much easier to generate lift on Earth than it is on Mars, clearly due to the fact of density.

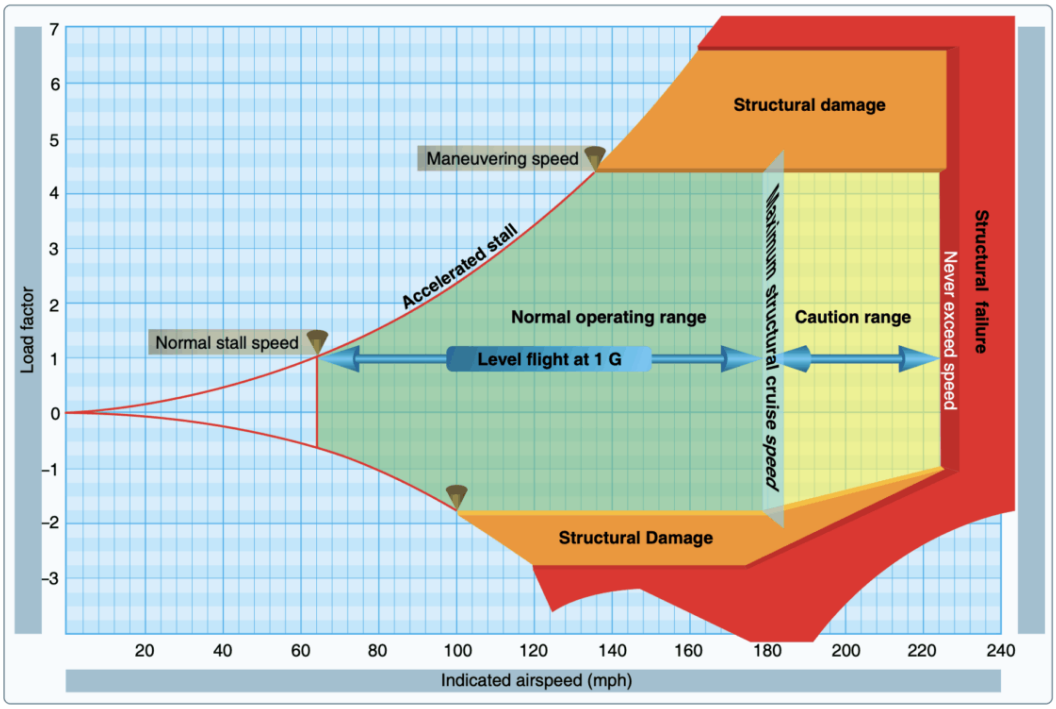

Figure 14: Generic Flight Envelope for reference.

In the Martian atmosphere, the flight envelope differs slightly from that on Earth. For this example, the aircraft is assumed to weigh 25 kilograms, with atmospheric conditions as described previously in Table BLANK. Calculations show that the maximum speed is primarily limited by the battery's capacity. Most UAVs are constructed from aluminum, which has a yield strength of approximately 40 megapascals. [9] Due to this high material strength, structural limitations are not a concern. However, typical UAV batteries can produce only up to 3000 watts, making the velocity limitations solely dependent on the battery. The flight envelope for operations on Mars is illustrated below in Figure 14.

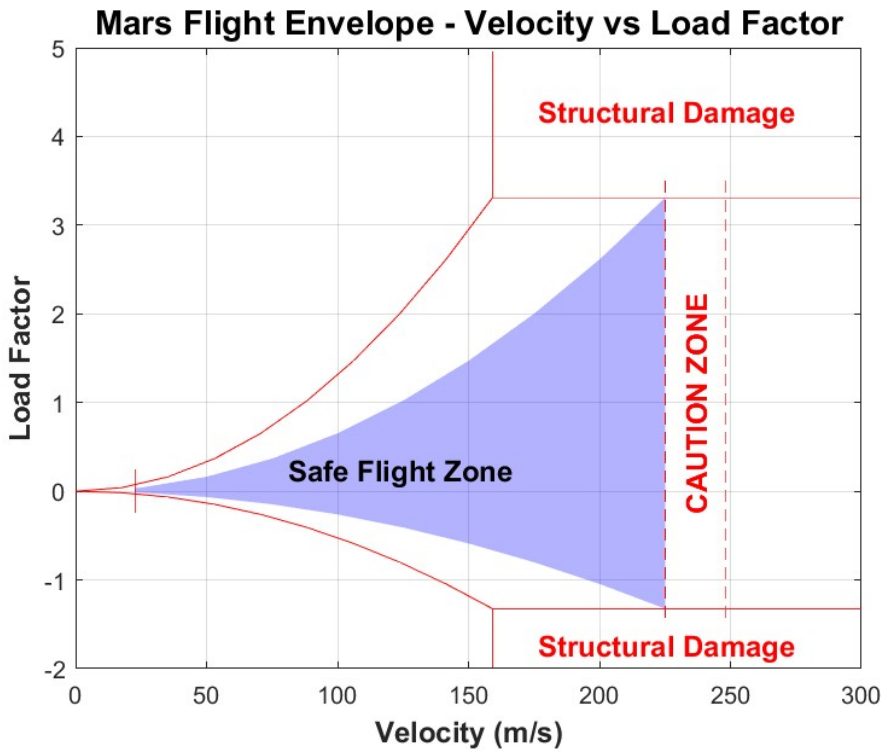

Figure 15: Theoretical Constructed Flight Envelope for Mars

In the flight envelope, the first set of dashed lines represents the battery's limitations, with the maximum velocity estimated to be around 225 meters per second. The caution zone indicates a range of varying battery power and efficiency, where the battery may produce more than the nominal 3000 watts. [10] Beyond the caution zone, at the second dashed line, the velocity limit is set at approximately 250 meters per second to account for these variations in battery performance.

The structural damage zones correspond to load factors high enough to cause deformation in the blade. The onset of this zone depends on the material properties, occurring sooner or later based on the material's yield strength. Structural damage does not necessarily indicate complete failure but rather that the wings are beginning to deform, making lift forces and vibratory behavior less predictable. This flight envelope produced is is primarily for level flight. The airfoil will experience greater load factors during High-G Maneuvers, but since this is a UAV it is unlikely to be required unless a strong storm blows through.

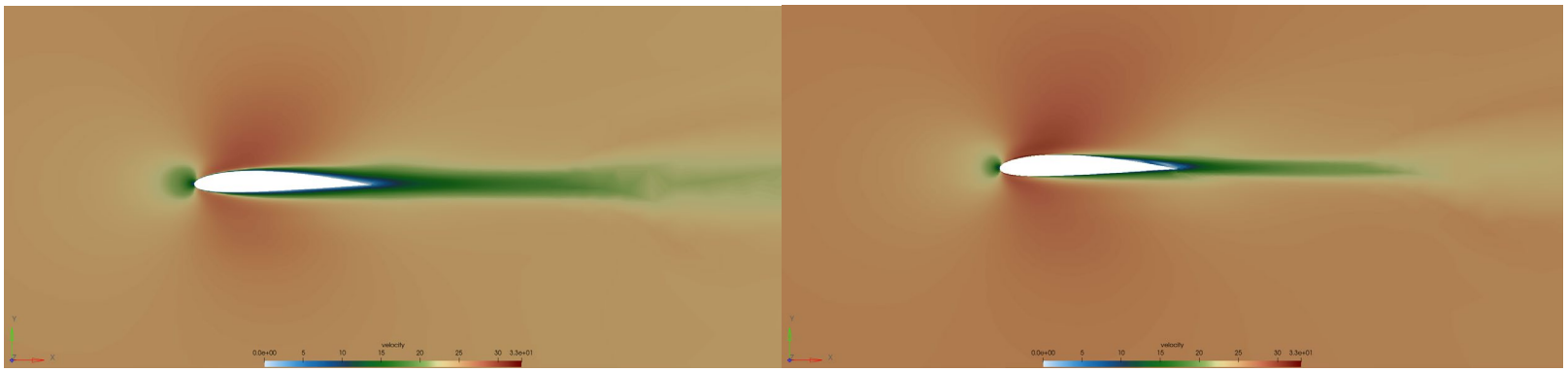

Figure 16: Comparison of the Mars (Left) and Earth (Right) at Minimum Mars Flight Speed 27 meters per second

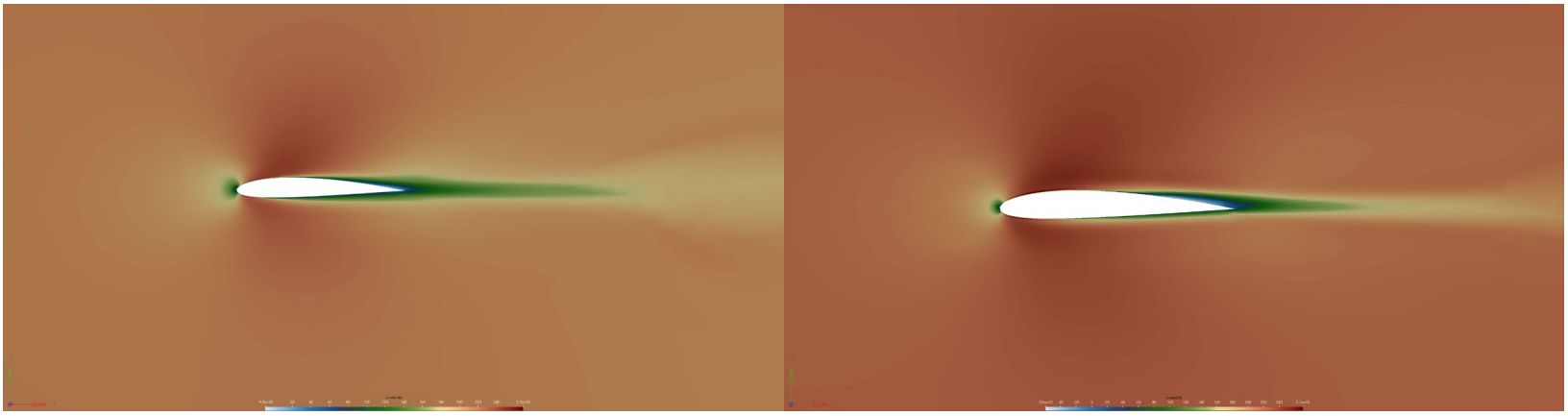

Figure 17: Comparison of the Mars (Left) and Earth (Right) at Minimum Mars Flight Speed 225 meters per second

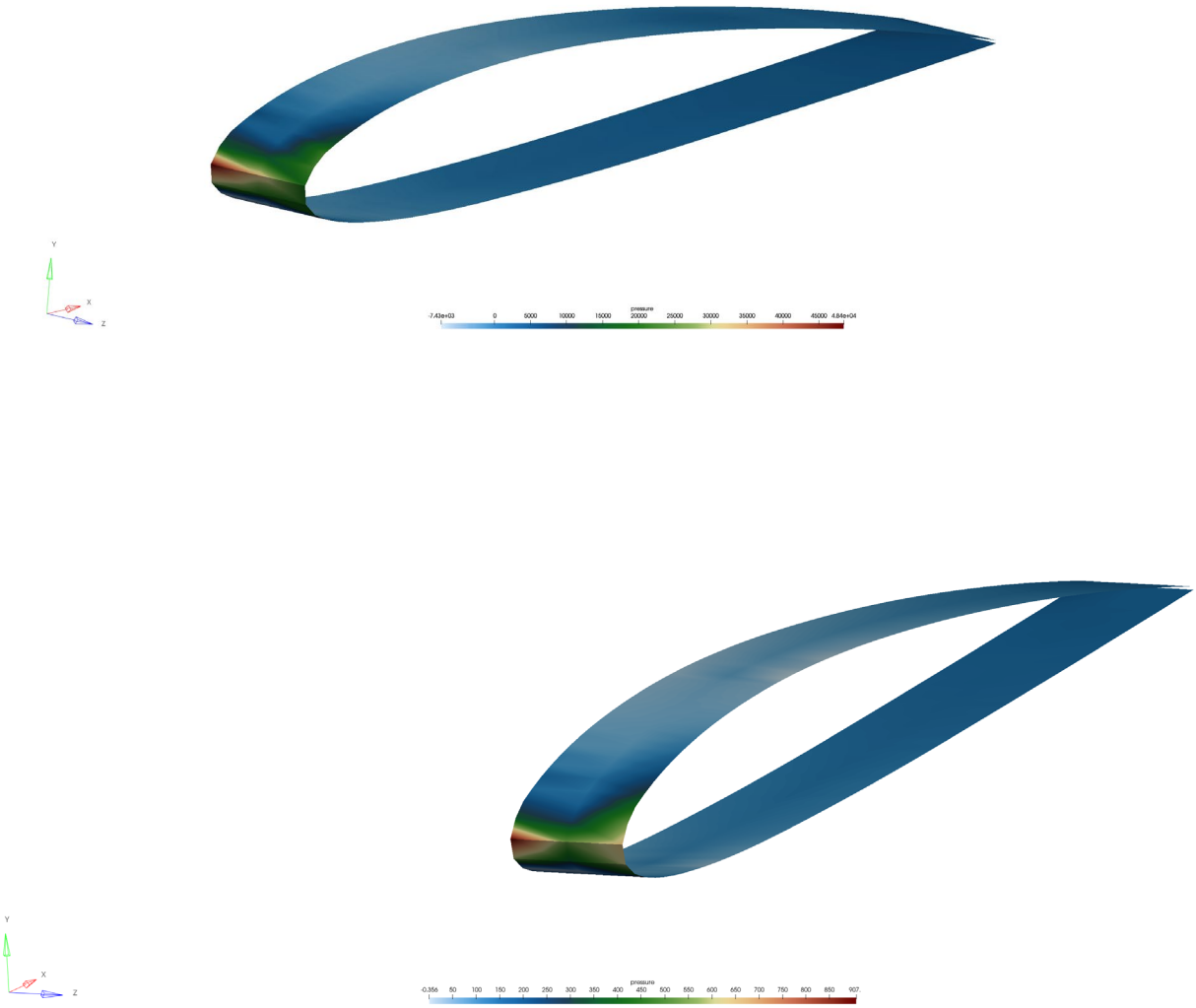

Figure 18: Comparison of the Mars (Below) and Earth (Above) Pressure on Airfoil tip at Maximum Mars Flight Speed 225 meters per second

We chose these pressure depictions at the high end of the speed threshold to see how much each differs. You can clearly see, based on the atmospheric differences that Earth experiences pressures on airfoil tips at a scale of at least 50 times more than on Mars, again expected from the difference in density values of the air. The air gathers quickly at the tips of the airfoil, and if the structure is not up to snuff, it will deform or fail completely due to this massive amount of pressure on the structure. Flight on Mars, in normal conditions yields more friendly results at a value of 900 Pa, compared to the high end Earth 48,000 Pa.

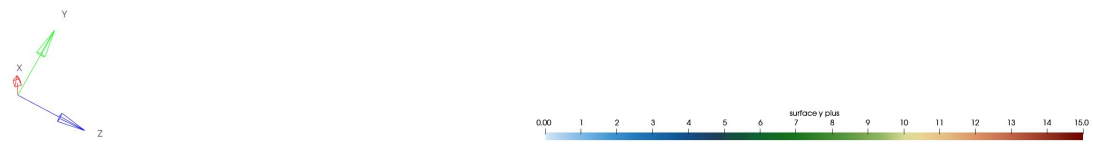
Y
X
Z
surface y plus
0.00
1
2
3
4
5
6
7
8
9
10
11
12
13
14
15.0

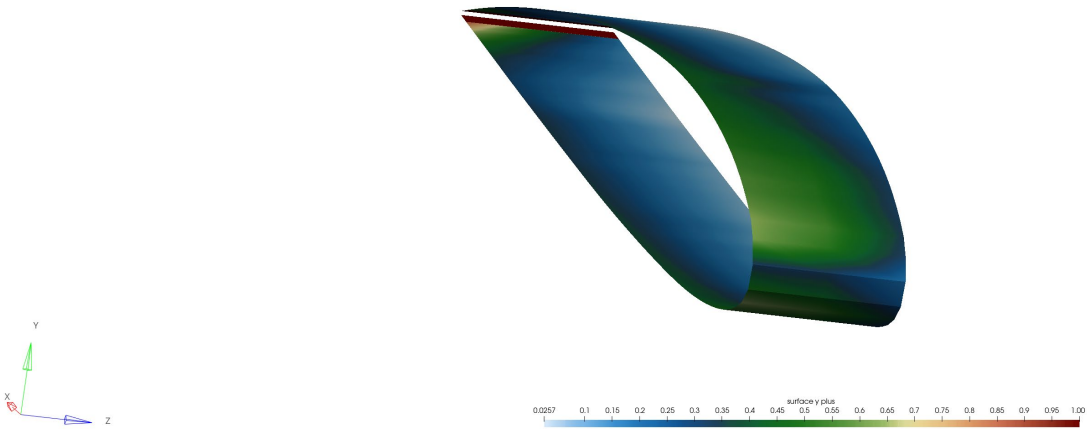

Figure 19: Comparison of the Mars (Below) and Earth (Above) surface y plus on Airfoil at Maximum Mars Flight Speed 225 meters per second

We chose these plots of the surface y+ values again at the maximum speed to see how the turbulence behaves. In truth, the insight here is not very evident and more analysis is required. The scale had to be chosen in order to see the true difference in the gradient of the surface y+ on the airfoil. We can see that the Earth airfoil depicted above experiences a greater spread of surface y+ treatment indicative of its higher Reynolds number compared to its Mars counter part. However, each airfoil experiences a very high amount of surface y+ up to the thousands, again to generalize the effect a smaller scale was chosen.

After testing the NACA 2412 airfoil at the minimum flight speed on Mars (27 meters per second) in both Martian and Earth atmospheres, a clear difference in trailing vortex behavior was observed. On Mars, the trailing vortex extends significantly farther than on Earth. This is likely due to the difference in atmospheric density; the reduced density on Mars slows the dissipation of the vortex compared to Earth's denser atmosphere.

On Earth, the flight envelope for a similar vehicle differs significantly from that on Mars, as shown in Figure BLANK. The minimum flight speed decreases to 18.7 meters per second, aligning with previously established data. At lower speeds, flight on Mars is more

challenging due to the higher coefficient of drag relative to the coefficient of lift, requiring a faster speed to overcome drag.

The safe flight zone is noticeably smaller, spanning only from 18.7 to 57 meters per second, primarily due to battery limitations. The assumed battery capacity of 3000 watts produces less thrust on Earth because of the increased air density and higher coefficient of drag. The caution zone extends up to 163 meters per second because, unlike on Mars, the vehicle on Earth is ultimately limited by the drag it produces at higher speeds. This flight envelope is consistent with UAVs like the RQ-7 Shadow UAV used by U.S. Military which has a recommend top speed of 130 mph 58 m/s.

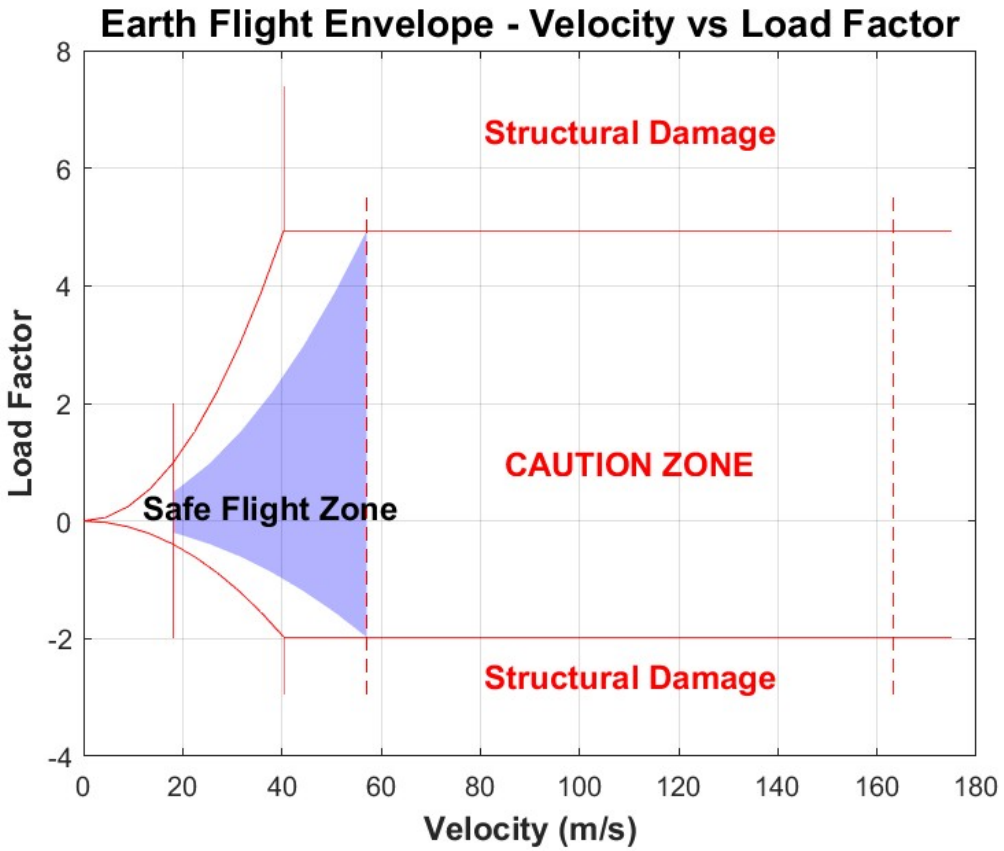

Figure 20: Theoretical Constructed Flight Envelope for Earth

The effects of the different atmospheres are evident in both the CFD models and the mathematically developed flight envelopes. Changes in air density influence the minimum and maximum flight speeds, the size of the safe flight and caution zones, and the extent of the wake produced by the airfoil.

3D Simulations (Run Set three)

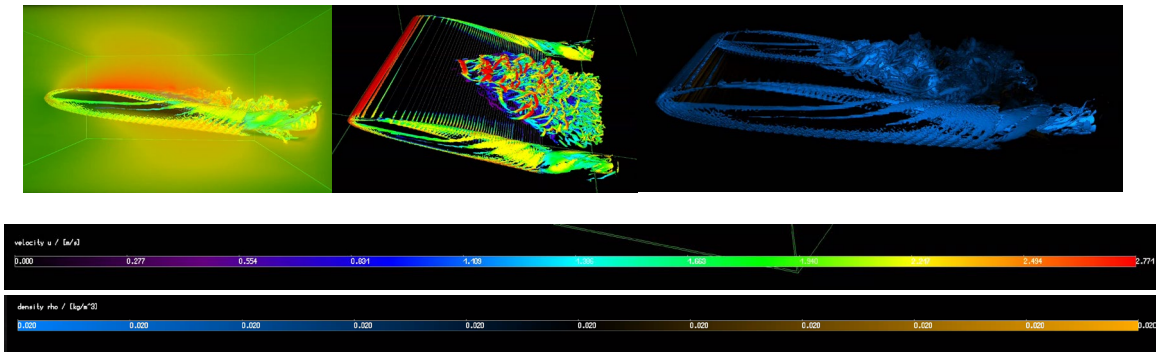

Figure 21: 3D Earth flight 2 m/s

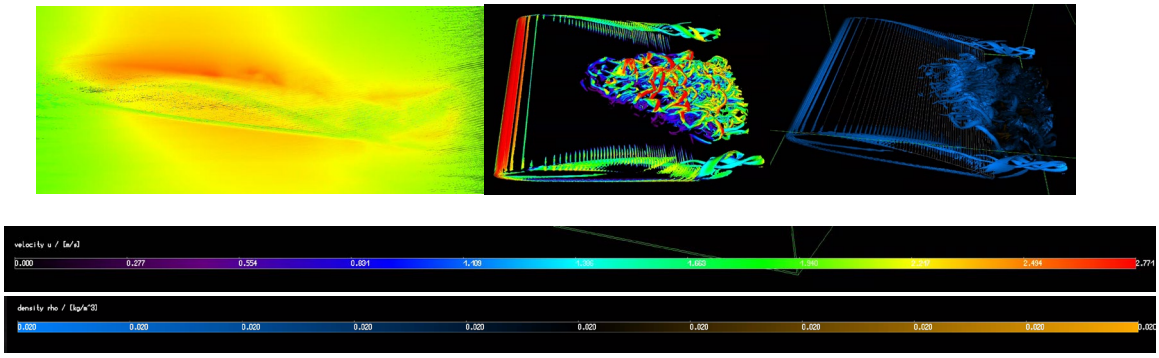

Figure 2214: 3D Martian flight 2 m/s

When comparing 3D simulations of the Martian and Earth atmospheres, the Martian atmosphere shows significantly fewer vortices at the edge of the airfoil and on its surface. However, as you can see, the flow's effect on the body is minimal. This is because the velocity in this case is less than 27 m/s, which is the minimum speed required according to the flight envelope.

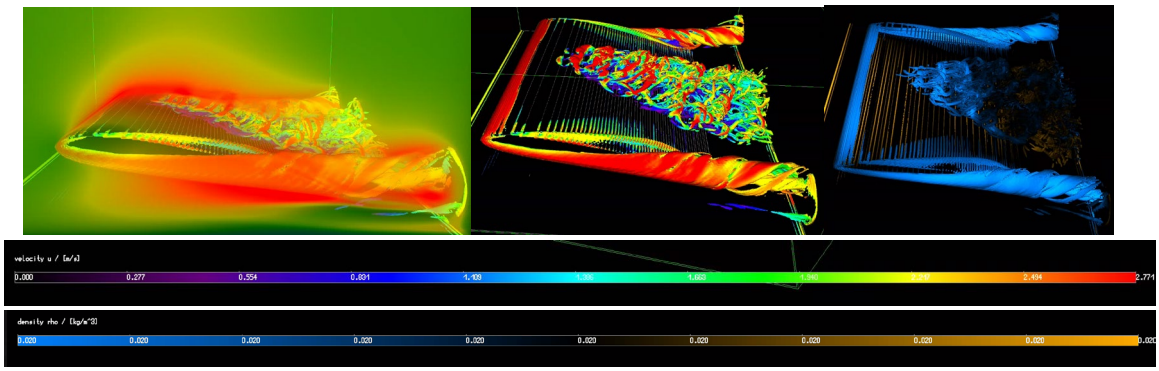

Figure 23: 3D Martian landing 2 m/s

During landing, the air bounces back from the ground, which is why we observe more vortices at the edge of the airfoil compared to flight conditions. Another contributing factor is that the velocity behavior near the ground surface is not the same as in the free stream.

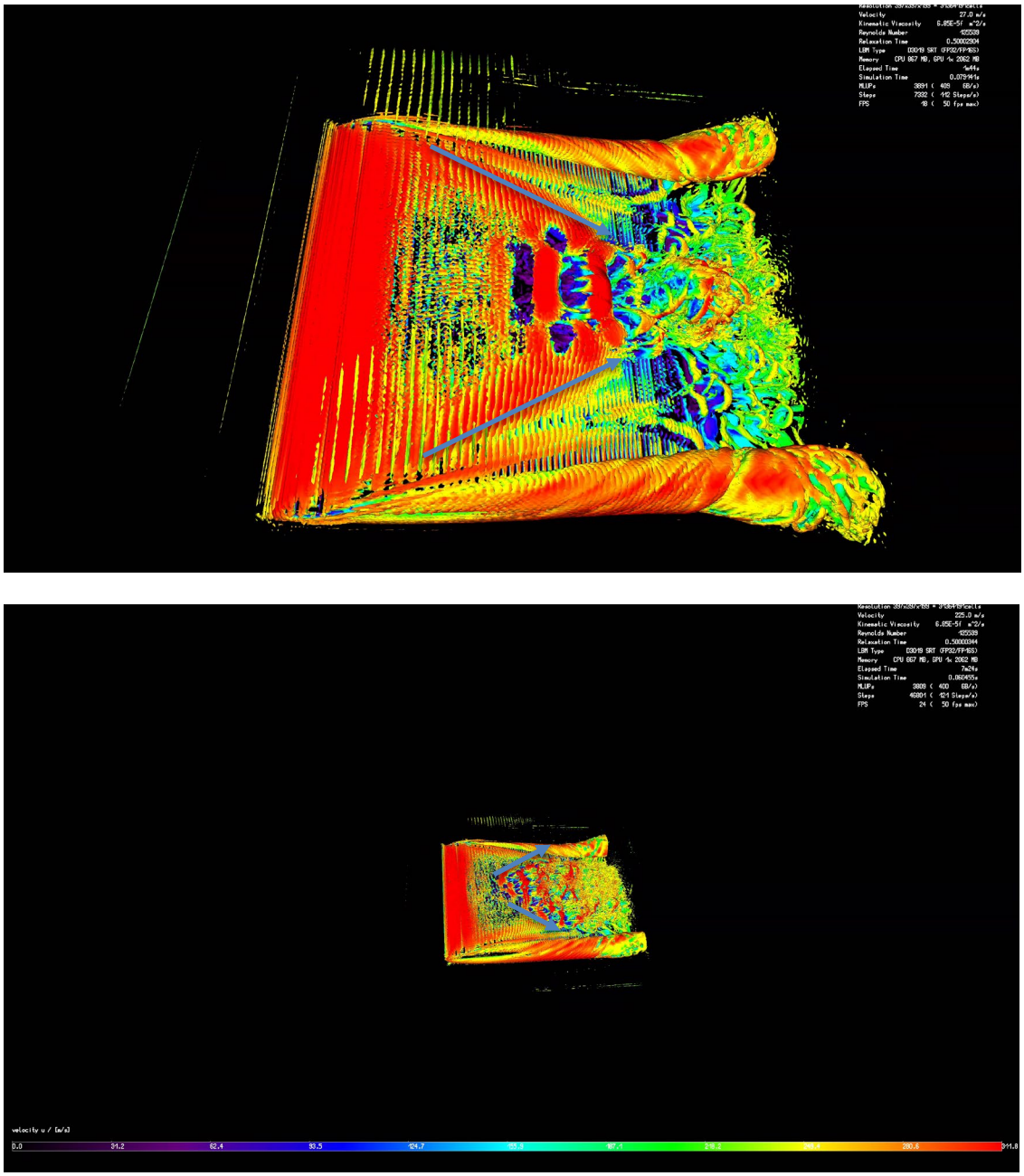

Figure 24: 3D simulation comparing 27 m/s and 225 m/s velocity

Overall, the flow behavior is less pronounced at the minimum and maximum speed limits of the flight envelope. However, when observing the top of the airfoil, the behavior is different. In the upper image, as shown at 27 m/s, the flow is converging, whereas at 225 m/s, the flow is diverging.

Section 6: Conclusions and Lessons Learned (Charles 33%, Batuhan 33%, Demetrius 33%)

Conclusions

The flow behavior differs significantly between the Martian and Earth atmospheres, primarily due to the drastic changes in the Reynolds number even at low speeds. These changes result in notable differences in flow characteristics. Analysis of the Cl and CD graphs reveals an interesting phenomenon: at very low speeds in the Martian atmosphere, CL is dominated by CD, whereas the opposite is true in Earth's atmosphere. This difference arises from the much lower air density on Mars, approximately 85% less than Earth's, reducing the airfoil's ability to generate lift. However, the viscosity on Mars is comparable to that of Earth, leading to increased skin friction and, consequently, greater drag.

At higher speeds, the behavior changes. For the same Reynolds number, an aircraft on Mars can achieve higher velocities than on Earth. These increased speeds enhance lift generation, improving flight efficiency and reducing fuel requirements for longer distances. When designing aircraft for Martian operations, modifications such as shorter wing spans or less cambered airfoils may be practical due to the ease of lift generation and transportation via rocket. Shorter wings reduce structural complexity and potential failure points. Additionally, with reduced moment forces, lighter and less robust materials can be used for the wings, simplifying construction and design.

To conclude, looking at flight in the Martian atmosphere has produced some intriguing results. The effect that angle of attack has on the coefficient of lift and drag seems to be similar regardless of atmospheric changes. The development of a flight envelope gave some insight into the limitations of flight in Martian atmosphere. Flight on Mars can be said to be significantly easier compared to Earth due to the ease of lift generation at moderate to high speeds. This advantage may allow for simpler wing designs that are better suited for Martian conditions. However, further analysis is required to assess additional factors such as the effects of extreme temperature fluctuations, dust storms on aerodynamic performance, material durability in the Martian environment, and the optimization of propulsion systems to account for the thinner atmosphere. These considerations will ensure the successful design and operation of aircraft for Martian missions.

Lessons Learned

The process from start to finish took time and teamwork to make even a minorly successful CFD model. The most critical components came down to building a model that reflected a geometry with tested values, an appropriately refined grid that balances computation time and detail and a strictly defined set of operating conditions to effectively compare results. Of all of the lessons, being able to prove that we have an accurate model in accordance with tested physics was the most important. We previously thought our model was relatively well represented given its rudimentary nature. However, upon further analysis of the data, there are still points of improvement to pursue. Our evaluation of the Coefficient of drag in no way clear way matched the accepted value, leading us to believe that an error in

geometry and possible case set up exists. This goes to show how critical it is to do this sort of benchmark testing to see if your model is in fact solving the correct problem.

Furthermore, while we see points of interest in the differences of the effects of the atmospheres on the airfoils, it's clear that further testing and validation is required to make a more accurate assessment. We've learned that it's critical to double over each other's analyses in order to ensure the correct approach is applied and that a more accurate conclusion is drawn. In essence, three engineers' brains are most certainly better than one.

References

[1] A. S. CNN, "Why Mars? The fascination with exploring the red planet," *CNN*, Apr. 15, 2021. https://www.cnn.com/2021/04/15/world/mars-exploration-humankind-scn/index.html

[2] NASA, "Mars 2020: Perseverance Rover - NASA Science," *science.nasa.gov*, 2020. https://science.nasa.gov/mission/mars-2020-perseverance/

[3] NASA, "Ingenuity Mars Helicopter - NASA Science," *science.nasa.gov*, 2024. https://science.nasa.gov/mission/mars-2020-perseverance/ingenuity-mars-helicopter/

[4] D. Dobrijevic, "Mars' Atmosphere: Composition, Climate & Weather," *Space.com*, Sep. 12, 2017. https://www.space.com/16903-mars-atmosphere-climate-weather.html

[5] National Aeronautics and Space Administration (NASA). 1993. "NACA 2412 Airfoil." Available online at https://ntrs.nasa.gov/citations/19930090976 (accessed September 18, 2024), page 38-40

[6] CFD 2024 - Google Drive

[7] Airfoil tools XFOIL Benchmark Data http://airfoiltools.com/polar/details?polar=xf-naca2412-il-100000

[8] UAV Navigation, "Flight Envelope | Support," *www.uavnavigation.com*, 2024. https://www.uavnavigation.com/support/kb/general/general-system-info/flight-envelope

[9] "Aluminum Alloys - Yield and Tensile Strength," *amesweb.info*. https://amesweb.info/Materials/Aluminum-Yield-Tensile-Strength.aspx

[10] G. Staff, "A Guide to Lithium Polymer Batteries for Drones," *Tyto Robotics*, Dec. 13, 2021. https://www.tytorobotics.com/blogs/articles/a-guide-to-lithium-polymer-batteries-for-drones